Light-Matter Interaction near the Schwinger Limit Using Tightly Focused Doppler-Boosted Lasers

Neïl Zaïm[1,*] Antonin Sainte-Marie[1] Luca Fedeli[1] Pierre Bartoli[1] Axel Huebl,[2]
Adrien Leblanc[3] Jean-Luc Vay[2] and Henri Vincenti[1,†]

[1]*Université Paris-Saclay, CEA, LIDYL, 91191 Gif-sur-Yvette, France*
[2]*Lawrence Berkeley National Laboratory, Berkeley, California 94720, USA*
[3]*LOA, CNRS, Ecole Polytechnique, ENSTA Paris, Institut Polytechnique de Paris, Palaiseau, France*

Strong-field quantum electrodynamics (SF QED) is a burgeoning research topic dealing with electromagnetic fields comparable to the Schwinger field ($\approx 1.32 \times 10^{18}$ V/m). While most past and proposed experiments rely on reaching this field in the rest frame of relativistic particles, the Schwinger limit could also be approached in the laboratory frame by focusing to its diffraction limit the light reflected by a plasma mirror irradiated by a multipetawatt laser. We explore the interaction between such intense light and matter with particle-in-cell simulations. We find that the collision with a relativistic electron beam would enable the study of the nonperturbative regime of SF QED, while the interaction with a solid target leads to a profusion of SF QED effects that retroact on the interaction. In both cases, relativistic attosecond pair jets with high densities are formed.

Multipetawatt femtosecond lasers [1] can nowadays reach intensities exceeding 10^{23} W/cm² [2], which are so high that strong-field quantum electrodynamics (SF QED) phenomena [3–5] are expected to come into play in laser-matter interactions. The dominant SF QED processes [6] are the discretized emission of high-energy photons by electrons [7] and the decay of high-energy photons into electron-positron pairs (nonlinear Breit-Wheeler [7,8]) in the presence of a strong field. These processes appear when the ratio χ between the electric field in the rest frame of a particle and the critical field of SF QED, the so-called Schwinger field [9] $E_S \approx 1.32 \times 10^{18}$ V/m, approaches unity. In the coming years, laser-electron collisions, a configuration that maximizes the χ parameter, should finally allow the study of these basic SF QED processes with $\chi > 1$ [10–14].

Going further, some of the most attractive prospects of SF QED are (i) the access to its fully nonperturbative regime, conjectured to occur when $\chi \gtrsim 1600$ [15], and for which there is no established theory [16–18], (ii) the exploration of QED-plasma states [19,20], defined by the self-consistent interaction between SF QED processes and plasma physics, which are relevant for understanding the environment of compact astrophysical objects (black holes, neutron stars) [21–24], and (iii) the possibility to develop novel sources of antimatter and photons with applications to high-energy physics or photonuclear science [25,26]. Unfortunately, these prospects should remain unattainable with usual laser-matter interaction scenarios (laser-electron collisions [10,27], seeded laser-laser collisions [28–30] and laser-solid interactions [31,32]) until the advent of lasers with power exceeding 10 PW [19] (although it should be noted that the first QED-plasma effects could be detected in the collision between a multipetawatt laser and a dense electron beam [27] and that the onset of the QED-plasma regime could be accessed during the interaction between a tightly focused 10 PW laser and a solid target [32]). Consequently, several alternative approaches are being investigated to probe SF QED more efficiently with existing laser facilities [33–35].

Among these, the possibility of boosting the intensity of a petawatt laser through its interaction with a solid target (that is ionized into a plasma mirror) has received significant attention [36–43]. During this interaction, two processes result in a strong intensification of the reflected laser. (i) First, the incident field drives relativistic oscillations of the plasma mirror surface. These oscillations periodically compress the incident laser energy in the form of a train of attosecond pulses by Doppler effect. In the spectral domain, this periodic compression is associated with a Doppler high-harmonic spectrum of the incident laser frequency [44,45]. (ii) The plasma mirror surface is carved into a paraboliclike mirror by the incident laser radiation pressure [46]. The resulting curvature leads to a focusing of the reflected laser down to much smaller focal volumes than possible with the incident laser frequency.

Particle-in-cell (PIC) [47] simulations have demonstrated that this spatiotemporal compression of the laser is associated with intensity gains that can exceed 3 orders of magnitude [39]. It was recently shown that the newly accessible 10^{24}–10^{26} W/cm² intensity range could be
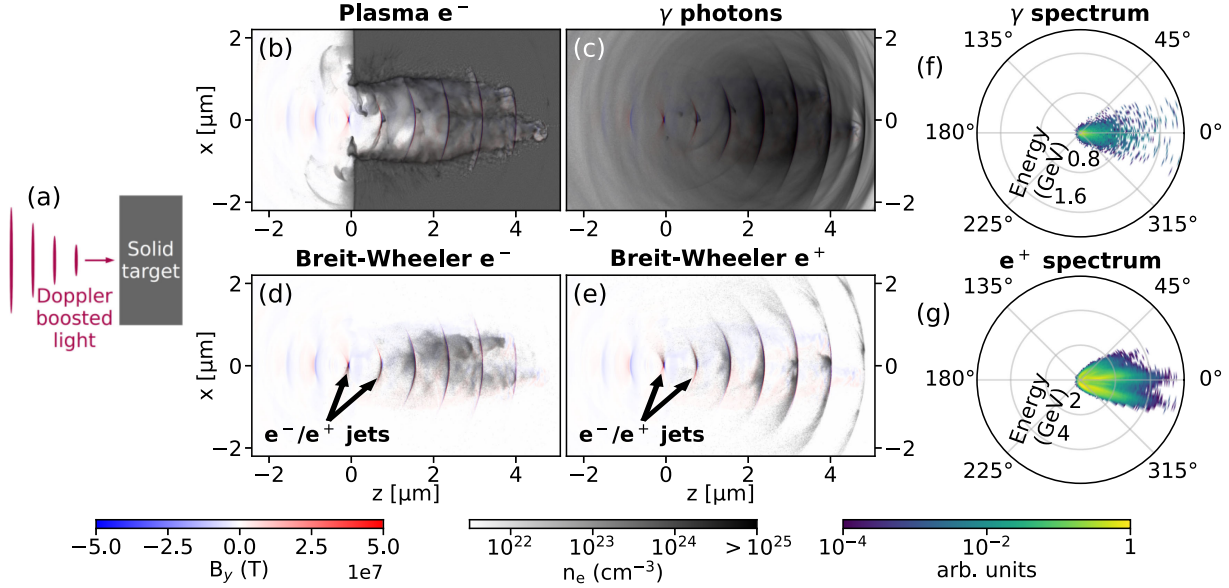
FIG. 1. Interaction between a boosted laser with 1.2×10^{28} W/cm^2 peak intensity and a solid target. (a) Schematic illustration. (b)–(e) Laser magnetic field combined with (b) the plasma electron, (c) the γ photon, (d) the Breit-Wheeler electron, or (e) the Breit-Wheeler positron density. (f),(g) γ photon (f) and positron (g) angularly resolved spectrum at the end of the simulation. See also Supplemental Material, Movies 1–3 [54].

leveraged to strongly increase the signatures of SF QED processes in laser-solid interactions [41].

Yet, the most appealing perspective opened by the Doppler boosting technique is the possibility to attain intensities between 10^{27} and 10^{29} W/cm^2 with the most powerful lasers available [40]. Reaching such intensities requires the boosted lasers to be focused close to their diffraction limit, which is challenging given the spatial scales involved (≈ 50 nm). Nevertheless, schemes are being explored to focus boosted lasers as tightly as possible [48], either by tuning the laser-plasma interaction or with external extreme ultraviolet optics, with the objective of approaching the Schwinger field (which corresponds to an intensity of 4.65×10^{29} W/cm^2) in the laboratory frame.

In this context, this letter aims at understanding the basic physics of laser-matter interactions with aberration-free Doppler boosted lasers focused close to their diffraction limit at intensities between 10^{27} and 10^{29} W/cm^2. This idealized scenario is an important first step to understand the main physical regimes coming into play in such conditions and help define and motivate future research directions with Doppler-boosted lasers.

To this end, we have performed 2D PIC simulations, using the code WarpX [49–51] coupled to the PICSAR QED library [52], of the two most common *single-laser* scenarios that are envisioned to probe SF QED: the interaction with a solid target, illustrated in Fig. 1(a) and the collision with a relativistic electron beam, illustrated in Fig. 2(a). We use the standard QED PIC method [6], combined with a particle thinning algorithm [53] to deal with the copious particle creation at such intensities.

We consider simple interaction geometries. The interaction with a solid is performed at normal incidence with a fully ionized SiO$_2$ target of constant density 6.5×10^{23} cm^{-3}. The collision with an electron beam is performed using beam parameters that are expected to become available soon in compact laser wakefield acceleration facilities [64]: an electron energy of 10 GeV and a charge of 10 pC spread in a 4 μm transverse size and a 6 μm longitudinal size. A 45° angle is used between the laser and the electrons with the aim of reducing radiative losses in the first cycles of the laser [65].

Finally, we use the same procedure as in Ref. [42] to model an ideal Doppler boosted laser: its spectrum comes from optimized PIC simulations and its spatiotemporal profile is obtained by assuming a diffraction-limited focusing of each frequency. With the chosen spectrum, wavelengths ranging between 8 and 800 nm significantly contribute to the peak intensity. The most intense attosecond pulse has, at focus, a duration of 21 attoseconds and a width of 39 nm in FWHM of the field. We have considered peak intensities between 1.3×10^{27} W/cm^2 and 1.2×10^{29} W/cm^2, which corresponds to primary laser powers ranging between 0.4 PW and 17 PW (on target) according to first estimates of the achievable intensity gains with the Doppler boosting technique in the diffraction limited regime [40]. Simulation details are given in Supplemental Material [54].

Figure 1 summarizes the main features of the interaction between a 1.2×10^{28} W/cm^2 boosted laser and a solid target. We note that the plasma is underdense for the high-frequency components of the laser. Combined with
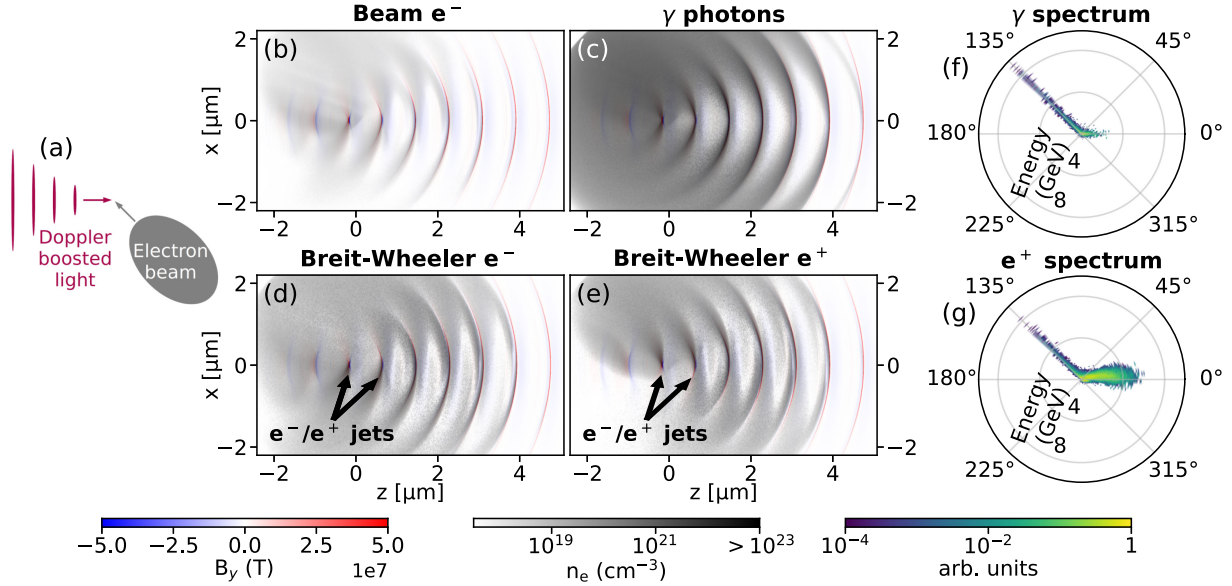
FIG. 2. Collision between a boosted laser with 1.2×10^{28} W/cm^2 peak intensity and a counterpropagative 10 GeV electron beam. (a) Schematic illustration. (b)–(e) Laser magnetic field combined with (b) the beam electron, (c) the γ photon, (d) the Breit-Wheeler electron, or (e) the Breit-Wheeler positron density. (f),(g) γ photon (f) and positron (g) angularly resolved spectrum at the end of the simulation. See also Supplemental Material, Movie 4 [54].

relativistic transparency [66,67], this means that a significant fraction of the laser propagates inside the solid, digging a plasma channel nearly void of electrons. The strong fields associated with the laser and the plasma channel [68] lead to copious γ photon and electron-positron pair generation up to $\sim$4 μm inside the solid, at which point the laser is almost completely absorbed.

The combination of the laser E and $v \times B$ forces is strong enough to directly accelerate the generated pairs in the laser propagation direction to energies up to 6 GeV [see Fig. 1(g)], in a process called vacuum laser acceleration [69]. As they are accelerated, the particles remain trapped over long distances in a given phase of the laser. This trapping can only occur at positions for which the field is sufficiently strong, i.e., near the attosecond pulses of the Doppler-boosted laser. Each attosecond pulse thus acts as a snowplow that bunches the generated pairs into very small volumes (typically 10 nm long and 200 nm wide at laser focus), leading to the formation of a train of extremely dense (exceeding 10^{25} cm^{-3}) attosecond electron-positron jets, as illustrated in Supplemental Material, Movie 3 [54]. Such a bunching would not occur if a standard laser were used instead of a Doppler-boosted laser, as discussed in Supplemental Material [54]. The photon spectrum, shown in Fig. 1(f), bears the signature of this acceleration, since the highest energy photons ($\approx$1 GeV) are emitted along the laser propagation direction. Finally, we observe that the electron and positron populations are spatially separated by the plasma channel fields [70], which are attractive for electrons and repulsive for positrons.

A similar simulation overview is shown in Fig. 2 for the collision with an electron beam. We observe that the laser is intense enough to put a large fraction of the 10 GeV electrons to a complete stop, by a combination of quantum Compton scattering and Lorentz force. The stopped electrons and the pairs that they generate are subsequently accelerated and bunched by the laser into relativistic jets. The formation of these dense jets thus appears to be a generic feature of Doppler-boosted laser-matter interactions close to the Schwinger limit. The electron and positron populations are again spatially separated, this time because of the asymmetric temporal profile of the boosted laser (see Supplemental Material [54]), which tends to push positrons or electrons in the positive or negative x direction.

The spectra displayed in Figs. 2(f) and 2(g) reveal that the particles are separated in two populations. The first one is made of particles that have not been stopped by the laser and travel along the initial electron beam direction. These particles can have very high energies, up to a 10 GeV cutoff corresponding to the initial electron energy. The second population is made of particles accelerated by the laser along its propagation direction and the photons that they emit. While the charged particles can be accelerated to multi-GeV energies, the γ photons of this population have rather low energies. This is because ultrarelativistic leptons copropagating with the laser have low χ parameters, which prevents the emission of high-energy photons. Although all particles see the strong laser field, these two populations coexist due both to the stochastic nature of the quantum interaction and to the fact that particles at different positions in the beam interact with fields of different strengths. This point is discussed in Supplemental Material [54], which also shows that the relative importance between these two
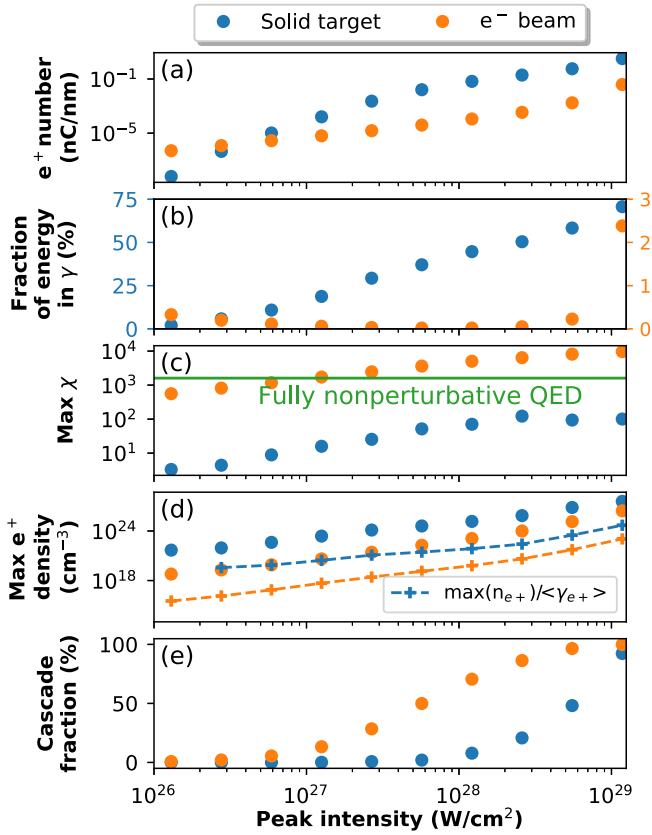
FIG. 3. Variation of selected quantities with boosted laser intensity for solid target (blue) and electron collision (orange) simulations. (a) Number of generated pairs. (b) Fraction of initial energy converted into γ photons. (c) Highest χ parameter reached by a target (solid or beam) electron. The nonperturbative QED threshold is shown in green. (d) Maximum positron density. The crosses show the maximum density divided by the average Lorentz factor of the positrons in the density peak. (e) Fraction of pairs originating from another Breit-Wheeler electron or positron.

populations changes drastically with laser intensity, as more particles are stopped and re-accelerated with stronger lasers.

Figure 3 provides a more quantitative view of the simulations, for different intensities. Panels (a) and (b) indicate that solid targets are more advantageous for maximizing the amount of SF QED processes, simply because the laser interacts with a large number of particles. For intensities exceeding 10^{27} W/cm^2, the number of generated pairs with a solid target is very high [typically in the nanocoulomb (nC) range] despite the small laser transverse size at focus (approximately 40 nm). Additionally, a very significant fraction of the laser energy (exceeding 50% for the highest intensities) is converted into γ photons. We are thus entering the QED-plasma regime [19], for which SF QED effects become coupled with the classical laser-plasma interaction. In particular, quantum emission of radiation eventually becomes the dominant absorption

mechanism, which may open the way toward advanced γ sources.

While a solid maximizes the amount of SF QED events, the main advantage of the collision with an electron beam is apparent in Fig. 3(c), which shows the maximum χ parameter reached in the simulations. The threshold for entering the nonperturbative regime of SF QED can be largely exceeded during the collision. These results demonstrate that radiation losses in the rising edge of the laser [65,71,72] do not necessarily preclude the exploration of the nonperturbative regime, even with a multiple cycle laser. In these simulations, the threshold is reached for intensities around 10^{27} W/cm^2. It should be kept in mind, however, that a more modest intensity of 10^{25} W/cm^2, which does not require a diffraction-limited focusing [39], would be enough to cross the threshold if a larger scale 100 GeV class conventional accelerator were used to generate the lepton beam, or alternately to reach χ values exceeding 100 and study deviations to the first-order expansion [73] if combined with a multi-GeV electron beam. Doppler boosting thus appears as a very promising solution for probing the nonperturbative limit of SF QED using existing laser technology.

A generic feature of the simulations is the formation of dense attosecond relativistic pair jets accelerated by the laser field. Figure 3(d) shows the peak density of these jets, which is higher with solid targets because the number of generated pairs is larger. Enormous densities are reached, up to 4×10^{27} cm^{-3} for the highest intensity, which is 5000 times the number density of the solid target itself. Such values are incomparably higher than those obtained experimentally by irradiating high-Z target, which are at most on the order of 10^{16} cm^{-3} [74,75], and even orders of magnitude higher than those obtained in simulations using 100 PW class lasers without Doppler boosting [28,29].

Relativistic pair jets can be found near neutron stars and black holes [24]. The interplay between pair plasma effects and SF QED is presumed to strongly impact the radiation emitted by these objects. Reproducing such jets in a laboratory could therefore prove valuable for understanding the signatures of extreme astrophysical objects, especially if pair plasma phenomena occur inside the laboratory-produced jets. A first criterion to assess whether such effects may occur is to compare the plasma period to the lifetime of the jets. In our simulations, the pairs typically reach their maximum density during only 1 fs, in which case this criterion [24] reads $n_{e+}/\gamma_{e+} \gg 1.5 \times 10^{20}$ cm^{-3}. The crosses of Fig. 3(d) indicate that this criterion is satisfied with solid targets above 10^{27} W/cm^2 and for electron beam collisions above 2×10^{28} W/cm^2. This is a first indication that pair plasma phenomena could occur in these jets.

Figure 3(e) shows the fraction of "cascade" pairs, defined as pairs generated from a Breit-Wheeler electron or positron (as opposed to pairs originating from a plasma

electron). With solid targets, the cascade fraction remains negligible below 10^{28} W/cm^2. This means that cascades are not necessary to obtain very high pair densities, which simply come from the bunching of the pairs by the laser.

As the intensity approaches the Schwinger limit, the emission of γ photons by particles accelerated by and copropagating with the laser, and the decay of these photons into new pairs becomes frequent enough to trigger avalanche-type cascades [4,76,77] that very quickly increase the density of the jets. At the highest intensities, these cascades start depleting the laser: in the solid target simulation with highest intensity, 75% of the energy of the strongest attosecond pulse is absorbed by the jet in its tail (including the photons in the jet) before the pulse even reaches the plasma surface. This is another example of retroaction of the SF QED effects on the laser-plasma interaction. At even higher intensities, the cascades develop so fast that the simulations could not be completed, for both the solid target and electron beam cases, because the pair plasma frequency became too high to be resolved, triggering a numerical plasma instability [47].

We finally remark that cascades appear at lower intensities in the electron beam simulations. This is due to conceptually different shower-type cascades [4,78]. Such cascades are driven by the high energy of the incident electrons, which leads to product particles that also have a high energy and can therefore create new particles themselves. However, the particle energy decreases at each generation of the cascade, which stops when the particle energies become too low or the particles exit the laser. The formation of shower and avalanche cascades is illustrated in Supplemental Material, Movies 4 and 5 [54].

In conclusion, we have explored the interaction of Doppler-boosted light with matter at intensities approaching the Schwinger limit. The collision with an electron beam emerges as a promising path to study the behavior of the basic single-particle SF QED processes in the regime $\chi \gg 1$, up to the nonperturbative limit of SF QED. The interaction with a solid target is a complementary strategy aimed at comprehending how these processes couple with large-scale classical electrodynamics and plasma phenomena. Such experiments could help validate commonly used SF QED modeling tools (the QED PIC method in particular), which would have significant implications for the understanding of the environment and signatures of extreme astrophysical objects. In both scenarios, Doppler-boosted laser matter interactions can serve as a source of ultradense pair jets, which could potentially mimic those existing next to black holes and neutron stars.

The richness of the physics glimpsed here should act as long-term motivation for experiments with Doppler boosted lasers focused as tightly as possible. Such a task will require extensive efforts to develop the new numerical tools that will be needed to model these interactions accurately, dealing with any common assumption that might break in these extreme conditions (at least radiative corrections should be included since χ values approach or exceed the nonperturbative threshold). Additionally, it will be important to identify, and hopefully mitigate potential experimental imperfections (laser or target) that could limit the achievable intensities with Doppler-boosted lasers.

[*]Corresponding author: neil.zaim@cea.fr
[†]Corresponding author: henri.vincenti@cea.fr

[1] C. N. Danson, C. Haefner, J. Bromage, T. Butcher, J.-C. F. Chanteloup, E. A. Chowdhury, A. Galvanauskas, L. A. Gizzi, J. Hein, D. I. Hillier *et al.*, High Power Laser Sci. Eng. **7**, e54 (2019).

[2] J. W. Yoon, Y. G. Kim, I. W. Choi, J. H. Sung, H. W. Lee, S. K. Lee, and C. H. Nam, Optica **8**, 630 (2021).

[3] A. Di Piazza, C. Müller, K. Z. Hatsagortsyan, and C. H. Keitel, Rev. Mod. Phys. **84**, 1177 (2012).

[4] A. Gonoskov, T. G. Blackburn, M. Marklund, and S. S. Bulanov, Rev. Mod. Phys. **94**, 045001 (2022).

[5] A. Fedotov, A. Ilderton, F. Karbstein, B. King, D. Seipt, H. Taya, and G. Torgrimsson, Phys. Rep. **1010**, 1 (2023).

[6] A. Gonoskov, S. Bastrakov, E. Efimenko, A. Ilderton, M. Marklund, I. Meyerov, A. Muraviev, A. Sergeev, I. Surmin, and E. Wallin, Phys. Rev. E **92**, 023305 (2015).

[7] T. Erber, Rev. Mod. Phys. **38**, 626 (1966).

[8] G. Breit and J. A. Wheeler, Phys. Rev. **46**, 1087 (1934).

[9] J. Schwinger, Phys. Rev. **82**, 664 (1951).

[10] M. Lobet, X. Davoine, E. d'Humières, and L. Gremillet, Phys. Rev. Accel. Beams **20**, 043401 (2017).

[11] J. M. Cole *et al.*, Phys. Rev. X **8**, 011020 (2018).

[12] K. Poder *et al.*, Phys. Rev. X **8**, 031004 (2018).

[13] H. Abramowicz *et al.*, arXiv:1909.00860.

[14] V. Yakimenko, L. Alsberg, E. Bong, G. Bouchard, C. Clarke, C. Emma, S. Green, C. Hast, M. J. Hogan, J. Seabury, N. Lipkowitz, B. O'Shea, D. Storey, G. White, and G. Yocky, Phys. Rev. Accel. Beams **22**, 101301 (2019).

[15] A. Fedotov, J. Phys. Conf. Ser. **826**, 012027 (2017).

[16] T. Podszus and A. Di Piazza, Phys. Rev. D **99**, 076004 (2019).

[17] A. Ilderton, Phys. Rev. D **99**, 085002 (2019).

[18] A. A. Mironov, S. Meuren, and A. M. Fedotov, Phys. Rev. D **102**, 053005 (2020).

[19] P. Zhang, S. S. Bulanov, D. Seipt, A. V. Arefiev, and A. G. R. Thomas, Phys. Plasmas **27**, 050601 (2020).

[20] G. Brodin, H. Al-Naseri, J. Zamanian, G. Torgrimsson, and B. Eliasson, Phys. Rev. E **107**, 035204 (2023).

[21] P. Meszaros, E. Ramirez-Ruiz, and M. J. Rees, Astrophys. J. **554**, 660 (2001).

[22] D. A. Uzdensky and S. Rightley, Rep. Prog. Phys. **77**, 036902 (2014).

[23] P. H. Bucksbaum, G. V. Dunne, F. Fiuza, S. Meuren, M. E. Peskin, D. A. Reis, G. Torgrimsson, G. White, and V. Yakimenko, *Probing QED Cascades and Pair Plasmas in Laboratory Experiments LoI to Cosmic Frontier*, Snowmass (2021).

[24] H. Chen and F. Fiuza, Phys. Plasmas **30**, 020601 (2023).

[25] M. Vranic, T. Grismayer, S. Meuren, R. A. Fonseca, and L. O. Silva, Phys. Plasmas **26**, 053103 (2019).

[26] Y.-J. Gu, M. Jirka, O. Klimo, and S. Weber, Matter Radiat. Extremes **4**, 064403 (2019).

[27] K. Qu, S. Meuren, and N. J. Fisch, Phys. Rev. Lett. **127**, 095001 (2021).

[28] E. N. Nerush, I. Y. Kostyukov, A. M. Fedotov, N. B. Narozhny, N. V. Elkina, and H. Ruhl, Phys. Rev. Lett. **106**, 035001 (2011).

[29] T. Grismayer, M. Vranic, J. L. Martins, R. A. Fonseca, and L. O. Silva, Phys. Plasmas **23**, 056706 (2016).

[30] X.-L. Zhu, T.-P. Yu, Z.-M. Sheng, Y. Yin, I. C. E. Turcu, and A. Pukhov, Nat. Commun. **7**, 13686 (2016).

[31] C. P. Ridgers, C. S. Brady, R. Duclous, J. G. Kirk, K. Bennett, T. D. Arber, A. P. L. Robinson, and A. R. Bell, Phys. Rev. Lett. **108**, 165006 (2012).

[32] C. P. Ridgers, C. S. Brady, R. Duclous, J. G. Kirk, K. Bennett, T. D. Arber, and A. R. Bell, Phys. Plasmas **20**, 056701 (2013).

[33] S. V. Bulanov, T. Esirkepov, and T. Tajima, Phys. Rev. Lett. **91**, 085001 (2003).

[34] A. Gonoskov, I. Gonoskov, C. Harvey, A. Ilderton, A. Kim, M. Marklund, G. Mourou, and A. Sergeev, Phys. Rev. Lett. **111**, 060404 (2013).

[35] A. Gonoskov, A. Bashinov, S. Bastrakov, E. Efimenko, A. Ilderton, A. Kim, M. Marklund, I. Meyerov, A. Muraviev, and A. Sergeev, Phys. Rev. X **7**, 041003 (2017).

[36] S. Gordienko, A. Pukhov, O. Shorokhov, and T. Baeva, Phys. Rev. Lett. **94**, 103903 (2005).

[37] B. Dromey, D. Adams, R. Hörlein, Y. Nomura, S. G. Rykovanov, D. C. Carroll, P. S. Foster, S. Kar, K. Markey, P. McKenna, D. Neely, M. Geissler, G. D. Tsakiris, and M. Zepf, Nat. Phys. **5**, 146 (2009).

[38] A. A. Gonoskov, A. V. Korzhimanov, A. V. Kim, M. Marklund, and A. M. Sergeev, Phys. Rev. E **84**, 046403 (2011).

[39] H. Vincenti, Phys. Rev. Lett. **123**, 105001 (2019).

[40] F. Quéré and H. Vincenti, High Power Laser Sci. Eng. **9**, e6 (2021).

[41] L. Fedeli, A. Sainte-Marie, N. Zaim, M. Thévenet, J. L. Vay, A. Myers, F. Quéré, and H. Vincenti, Phys. Rev. Lett. **127**, 114801 (2021).

[42] A. Sainte-Marie, L. Fedeli, N. Zaïm, F. Karbstein, and H. Vincenti, New J. Phys. **24**, 065005 (2022).

[43] M. Marklund, T. G. Blackburn, A. Gonoskov, J. Magnusson, S. S. Bulanov, and A. Ilderton, High Power Laser Sci. Eng. **11**, 1 (2023).

[44] U. Teubner and P. Gibbon, Rev. Mod. Phys. **81**, 445 (2009).

[45] C. Thaury and F. Quéré, J. Phys. B **43**, 213001 (2010).

[46] H. Vincenti, S. Monchocé, S. Kahaly, G. Bonnaud, P. Martin, and F. Quéré, Nat. Commun. **5**, 3403 (2014).

[47] C. K. Birdsall and A. B. Langdon, *Plasma Physics via Computer Simulation* (CRC Press, Boca Raton, 2004).

[48] L. Chopineau, A. Denoeud, A. Leblanc, E. Porat, P. Martin, H. Vincenti, and F. Quéré, Nat. Phys. **17**, 968 (2021).

[49] A. Myers *et al.*, Parallel Comput. **108**, 102833 (2021).

[50] L. Fedeli, A. Huebl, F. Boillod-Cerneux, T. Clark, K. Gott, C. Hillairet, S. Jaure, A. Leblanc, R. Lehe, A. Myers, C. Piechurski, M. Sato, N. Zaim, W. Zhang, J.-L. Vay, and H. Vincenti, in *SC22: International Conference for High Performance Computing, Networking, Storage and Analysis* (2022), pp. 1–12, 10.1109/SC41404.2022.00008.

[51] https://github.com/ECP-WarpX/WarpX.

[52] L. Fedeli, N. Zaïm, A. Sainte-Marie, M. Thévenet, A. Huebl, A. Myers, J.-L. Vay, and H. Vincenti, New J. Phys. **24**, 025009 (2022).

[53] A. Muraviev, A. Bashinov, E. Efimenko, V. Volokitin, I. Meyerov, and A. Gonoskov, Comput. Phys. Commun. **262**, 107826 (2021).

[54] See Supplemental Material at http://link.aps.org/supplemental/10.1103/PhysRevLett.132.175002, which includes Refs. [55–63] for more details regarding the simulation parameters and the spatiotemporal profile of the Doppler boosted laser, and for movies illustrating the interactions and QED-cascade formation.

[55] B. B. Godfrey and J.-L. Vay, J. Comput. Phys. **248**, 33 (2013).

[56] H. Qin, S. Zhang, J. Xiao, J. Liu, Y. Sun, and W. M. Tang, Phys. Plasmas **20,** 084503 (2013).

[57] J.-L. Vay, I. Haber, and B. B. Godfrey, J. Comput. Phys. **243,** 260 (2013).

[58] G. Blaclard, H. Vincenti, R. Lehe, and J. L. Vay, Phys. Rev. E **96,** 033305 (2017).

[59] Kane Yee, IEEE Trans. Antennas Propag. **14,** 302 (1966).

[60] O. Shapoval, J.-L. Vay, and H. Vincenti, Comput. Phys. Commun. **235,** 102 (2019).

[61] A. Bourdier, Phys. Fluids **26,** 1804 (1983).

[62] J.-L. Vay, D. P. Grote, R. H. Cohen, and A. Friedman, Comput. Sci. Discovery **5,** 014019 (2012).

[63] H. Vincenti and J.-L. Vay, Comput. Phys. Commun. **228,** 22 (2018).

[64] F. Albert *et al.*, New J. Phys. **23,** 031101 (2021).

[65] T. G. Blackburn, A. Ilderton, M. Marklund, and C. P. Ridgers, New J. Phys. **21,** 053040 (2019).

[66] G. A. Mourou, T. Tajima, and S. V. Bulanov, Rev. Mod. Phys. **78,** 309 (2006).

[67] S. Palaniyappan, B. M. Hegelich, H.-C. Wu, D. Jung, D. C. Gautier, L. Yin, B. J. Albright, R. P. Johnson, T. Shimada, S. Letzring, D. T. Offermann, J. Ren, C. Huang, R. Hörlein, B. Dromey, J. C. Fernandez, and R. C. Shah, Nat. Phys. **8,** 763 (2012).

[68] D. J. Stark, T. Toncian, and A. V. Arefiev, Phys. Rev. Lett. **116,** 185003 (2016).

[69] M. Thévenet, A. Leblanc, S. Kahaly, H. Vincenti, A. Vernier, F. Quéré, and J. Faure, Nat. Phys. **12,** 355 (2015).

[70] A. Pukhov, Z.-M. Sheng, and J. Meyer-ter Vehn, Phys. Plasmas **6,** 2847 (1999).

[71] Y. Kravets, A. Noble, and D. Jaroszynski, Phys. Rev. E **88,** 011201(R) (2013).

[72] C. Baumann, E. N. Nerush, A. Pukhov, and I. Y. Kostyukov, Sci. Rep. **9,** 9407 (2019).

[73] A. Di Piazza, T. N. Wistisen, M. Tamburini, and U. I. Uggerhøj, Phys. Rev. Lett. **124,** 044801 (2020).

[74] E. Liang, T. Clarke, A. Henderson, W. Fu, W. Lo, D. Taylor, P. Chaguine, S. Zhou, Y. Hua, X. Cen, X. Wang, J. Kao, H. Hasson, G. Dyer, K. Serratto, N. Riley, M. Donovan, and T. Ditmire, Sci. Rep. **5,** 13968 (2015).

[75] G. Sarri *et al.*, Nat. Commun. **6,** 6747 (2015).

[76] A. R. Bell and J. G. Kirk, Phys. Rev. Lett. **101,** 200403 (2008).

[77] S. S. Bulanov, C. B. Schroeder, E. Esarey, and W. P. Leemans, Phys. Rev. A **87,** 062110 (2013).

[78] A. Mironov, N. Narozhny, and A. Fedotov, Phys. Lett. A **378,** 3254 (2014).